Supporting Information

Heteroatom-doped Carbon Nanosheets Decorated with FeS Nanoparticles for Efficient Bifunctional Oxygen Electrocatalysis

Yuhan Liu,[a] Jie Huang, [a] Long Chen, [a] Shuhang Fang, [a] Hanfei Xiong, [a] Xuejun Liu,*[a] Junyuan Xu*[b] and Lixue Zhang*[a]

[a] College of Chemistry and Chemical Engineering, Collaborative Innovation Center for Hydrogen Energy Key Materials and Technologies of Shandong Province, Qingdao University, Qingdao 266071, P. R. China. E-mail: xjliu@qdu.edu.cn, zhanglx@qdu.edu.cn

[b] Laboratory of Advanced Spectro-electrochemistry and Li-ion Batteries, Dalian Institute of Chemical Physics, Chinese Academy of Sciences, Dalian 116023, China. E-mail: junyuanxu@dicp.ac.cn

Materials: Sodium lignosulfonate (LS) was obtained from Aladdin Biochemical Technology Co., Ltd., Shanghai. Sulfuric acid (H_2SO_4), zinc acetate dihydrate ($Zn(CH_3COO)_2·2H_2O$), sodium chloride (NaCl) and iron(III) nitrate nonahydrate ($Fe(NO_3)_3·9H_2O$) were obtained from Sinopharm Chemical Reagent Co., Ltd. Melamine ($C_3H_6N_6$) and potassium hydroxide (KOH) were purchased from Macklin Biochemical Co., Ltd., Shanghai. 5% Nafion solution was purchased from Suzhou Sinero Technology Co., Ltd. Meanwhile, 20% platinum on graphitized carbon and ruthenium oxide (RuO_2) were obtained from Sigma-Aldrich Trading Co., Ltd., Shanghai. All chemical reagents applied in this experiment were directly used without further purification. The deionized (DI) water adopted in the present work was purified by an UPR-II-10T ultrapure water purification system.

Synthesis of FeS@NC： Firstly, 1 g sodium lignosulfonate and 4 g NaCl were dissolved into 40 mL DI water with continuous stirring. After complete dissolution, 1 g melamine and 0.5 mmol $Fe(NO_3)_3·9H_2O$ were added and the stirring was continued for 6 h to ensure the formation of homogeneous solution. The obtained mixture was rapidly frozen with liquid nitrogen and then freeze-dried at –60 °C under a vacuum of 7 Pa for 48 hours. The freeze-dried sample was ground by agate mortar to obtain fine powders. The dried powders were subjected to high-temperature annealing at 900 °C (heating rate of 5 °C min^{-1}) for 4 hours in an argon atmosphere. Finally, the obtained black powders were poured into a beaker, added with DI water and stirred for 48 h to wash away the excess NaCl template. No additional acid etching was required during the washing process. Then the mixture was subjected to suction filtration, and the resulting black powders were dried to obtain the final products. For comparison, FeS@NC with different annealing temperatures were synthesized using a procedure similar to above process except for adjusting the annealing temperature to 700 °C and 800 °C, respectively, and the prepared catalysts were denoted as FeS@NC-700 and FeS@NC-800. Following the same procedure, lignin-derived N-doped porous carbon (NC-900) was also synthesized without the addition of $Fe(NO_3)_3·9H_2O$ during the preparation with all other conditions unchanged.

Physical characterization: The nanostructure and morphology were characterized using the following equipment: SEM (ZEISS Sigma 300) and TEM (Talos F200X). A Micromeritics ASAP 2460 system was used for the measurement of Brunauer-Emmett-Teller (BET) specific

surface area and pore size distribution. XRD data were obtained from a Rigaku x-ray diffractometer. Surface chemistry and composition of samples were characterized by X-ray photoelectron spectroscopy (XPS) with a Thermo Scientific K-Alpha (monochromatic AI Kα source). An American Thermofisher DXR2 Raman spectrometer with incident laser wavelength of 532 nm was deployed for Raman measurements.

Electrochemical measurements

Oxygen reduction reaction (ORR): All electrochemical measurements were performed on a CHI 730 electrochemical workstation using a standard three-electrode configuration at ambient temperature. All potentials were referenced to the reversible hydrogen electrode (RHE) scale, following the conversion equation:

$$E_{RHE} = E_{Hg/HgO} + 0.059 \times pH + 0.098\,V \quad \text{.....(1)}$$

Current densities reported in this study were normalized to the geometric surface area of the glassy carbon electrode (GCE). A glassy carbon electrode (GCE, geometric area = 0.2475 cm^2, a graphene rod, and a Hg/HgO electrode served as the working, counter, and reference electrodes, respectively. Prior to use, the GCE was sequentially polished with 0.5 μm and 0.05 μm alumina slurries, then rinsed with deionized (DI) water and absolute ethanol to eliminate surface-adsorbed impurities.

The working electrode was fabricated as follows: 5 mg of the as-synthesized catalyst (or commercial 20 wt% Pt/C) was dispersed in 1 mL of a mixed solvent (DI water: absolute ethanol: 5.0 % Nafion solution = 16: 16: 1, v/v/v). The mixture was sonicated at 20 °C for 30 minutes to form a homogeneous catalyst ink. Subsequently, 10 μL of the homogeneous ink was drop-cast onto the polished GCE surface and air-dried, yielding a catalyst mass loading of 0.202 mg cm^{-2}. Oxygen reduction reaction (ORR) performance was evaluated in 0.1 M KOH electrolyte saturated with either O_2 or N_2. Cyclic voltammetry (CV) measurements were conducted at scan rates ranging from 20 to 100 mV s^{-1}. Linear sweep voltammetry (LSV) measurements were performed using a rotating disk electrode (RDE) at rotation speeds of 400–2500 rpm. The stability of the prepared catalyst and commercial Pt/C was assessed via chronoamperometry (CA) in O_2-saturated electrolyte at 0.5 V vs. RHE. For the methanol

tolerance test, 1 M methanol was introduced into the O_2-saturated electrolyte at ~500 s, and the current response was monitored at 0.565 V *vs*. RHE.

For rotating ring-disk electrode (RRDE) measurements, the Pt ring potential was held at 1.4 V vs. RHE in 0.1 M KOH. The number of transferred electrons (n) and the percentage of hydrogen peroxide (H_2O_2) produced were calculated using the following equations:

$$n = 4 \times i_d/(i_d + i_r/N) \quad \text{.....(2)}$$

$$H_2O_2\ \% = (200 \times i_r/N)/(i_d + i_r/N) \quad \text{.....(3)}$$

Where i_d represents the current of disk electrode, i_r is the current of ring electrode and *N* is the collection efficiency of the ring electrode (0.37).

The number of transferred electrons was calculated using the Koutecky-Levich (K-L) equation:

$$1/J = 1/J_k + 1/J_L = 1/J_k + 1/(B\omega^{\frac{1}{2}}) \quad \text{.....(4)}$$

$$B = 0.62nFC_0D_0^{2/3}v^{-1/6} \quad \text{.....(5)}$$

where *J* is the measured current density, J_k is the kinetic diffiusionn density, ω is the electrode rotation rate, *n* is the electron transfer number, *F* is the Faraday constant of 96485 C mol^{-1}, C_0 is the bulk concentration of O_2 (1.2×10^{-3} mol cm^3 in 0.1 M KOH), D_0 represents the O_2 diffusion coefficient (1.9×10^{-5} cm^2 s^{-1} in 0.1 M KOH) and v is the kinetic viscosity of the electrolyte (0.01 cm^2 s^{-1} in 0.1 M KOH).

Oxygen evolution reaction (OER): All oxygen evolution reaction (OER) measurements for the catalysts were performed using a Bio-logic VSP-300 electrochemical workstation with a standard three-electrode configuration. A Hg/HgO electrode was used as the reference electrode, a graphite rod as the counter electrode, and a catalyst-loaded glassy carbon electrode (GCE) as the working electrode. The electrolyte was 1 M KOH solution. Linear sweep

voltammetry (LSV) curves were recorded in the potential range of 1.1–3 V (vs. RHE) at a scan rate of 5 mV s^{-1} without iR compensation. The measured potential relative to the reversible hydrogen electrode (RHE) was calculated using the formula $E_{RHE} = E_{Hg/HgO} + 0.059 \times pH + 0.098\,V$. The Tafel slope was determined from the linear sweep voltammetry (LSV) polarization curve.

***Assembly and test of aqueous Zn-air batteries*:** The catalyst ink was prepared by mixing 5 mg of catalyst powder, 485 μL of absolute ethanol, 485 μL of deionized water, and 30 μL of Nafion solution, followed by ultrasonication to achieve homogeneous dispersion. A piece of hydrophobic carbon paper (1 × 1 cm) was cut, and the ink was drop-cast onto the carbon paper, resulting in a catalyst loading of 1 mg cm^{-2}.The liquid Zn-air batteries (ZABs) were assembled using polished zinc foil as the anode, aqueous solution containing 6 M KOH + 0.2 M $Zn(CH_3COO)_2$ as the electrolyte, and FeS@NC-900 or commercial 20 wt% Pt/C+RuO_2 coated on carbon paper as the air cathode. The open circuit voltage, charge and discharge curves were measured using a CHI 730 electrochemical workstation. The power density, specific capacity, voltage platform and cyclic stability were measured using a LANBTS multi-channel system.

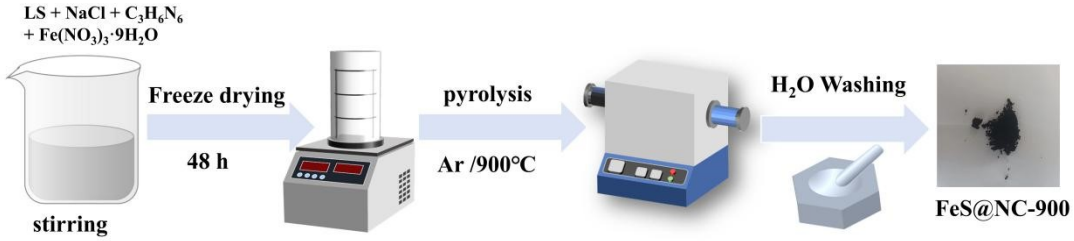

Figure S1. Schematic diagram of the synthesis for FeS@NC samples.

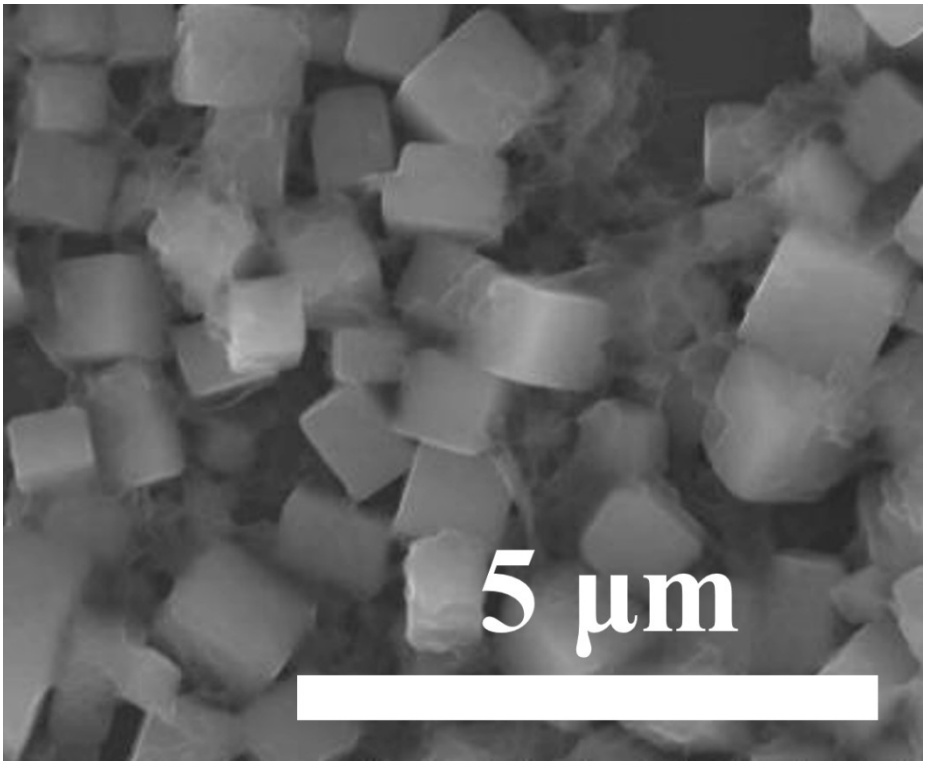

Figure S2. Scanning electron microscopy (SEM) image of Fe^{3+}/melamine/NaCl /lignosulfonate complex.

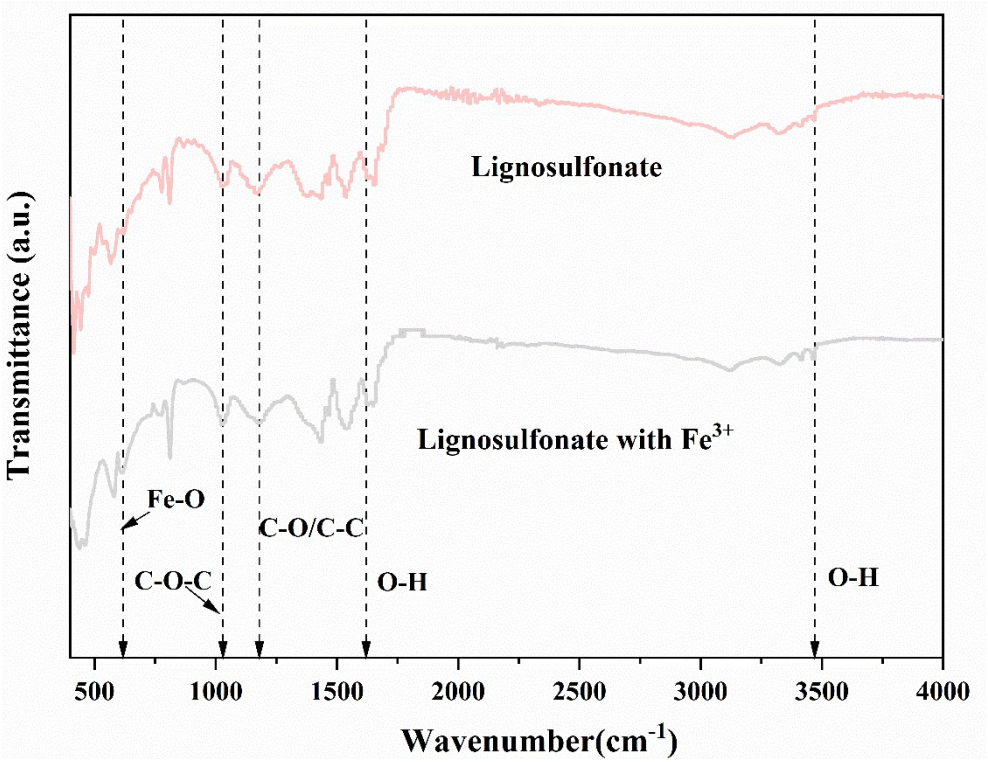

Figure S3. Fourier transform infrared (FT-IR) spectra for lignosulfonate and lignosulfonate coordinated with $Fe(NO_3)_3 \cdot 9H_2O$.

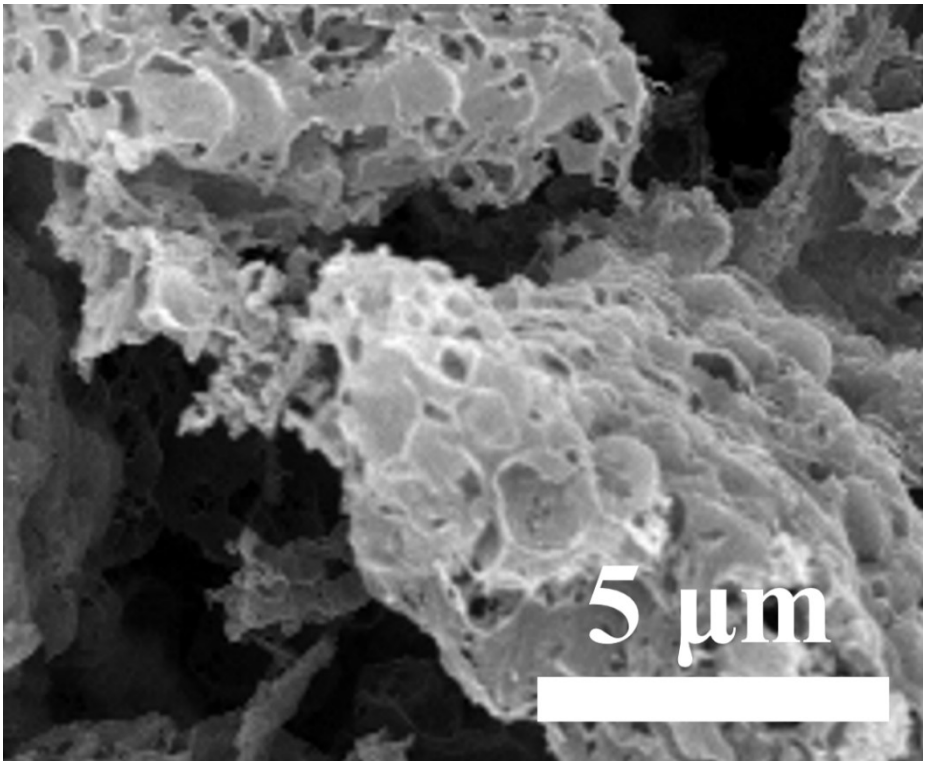

Figure S4. SEM image of the pyrolyzed products before water washing.

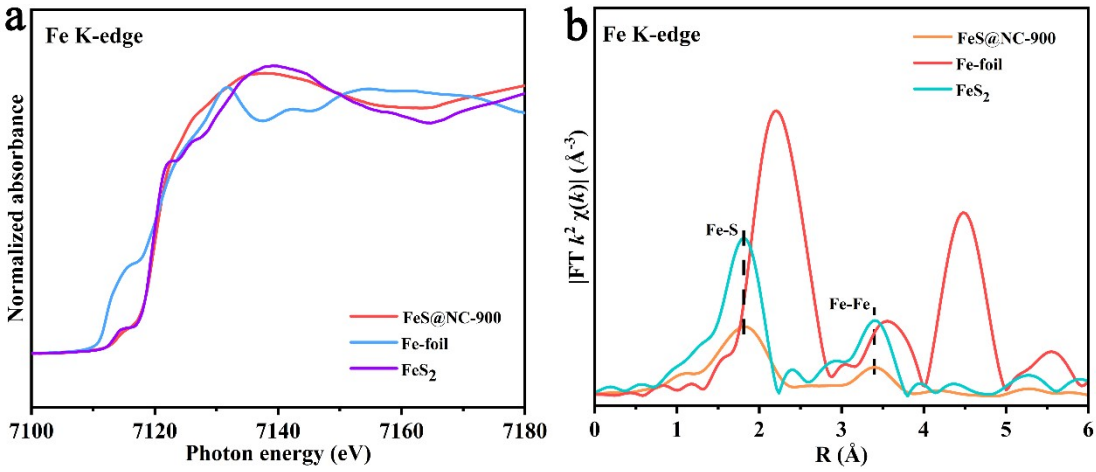

Figure S5. (a) Fe K-edge X-ray absorption near edge structure (XANES) spectra and (b) Fourier-transformed extended X-ray absorption fine structure (FT-EXAFS) spectra at the Fe K-edge.

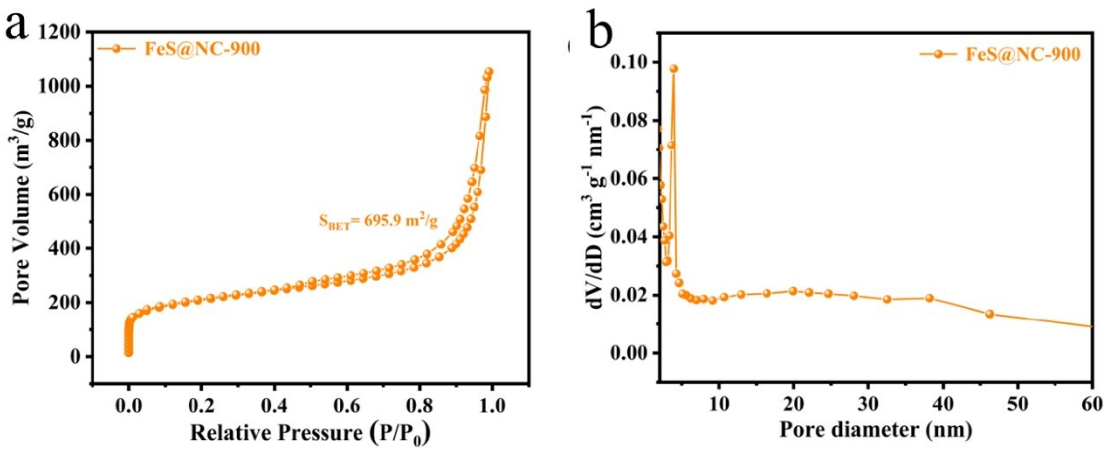

Figure S6. (a) Nitrogen adsorption–desorption isotherm and (b) the corresponding pore size distribution curve of FeS@NC-900.

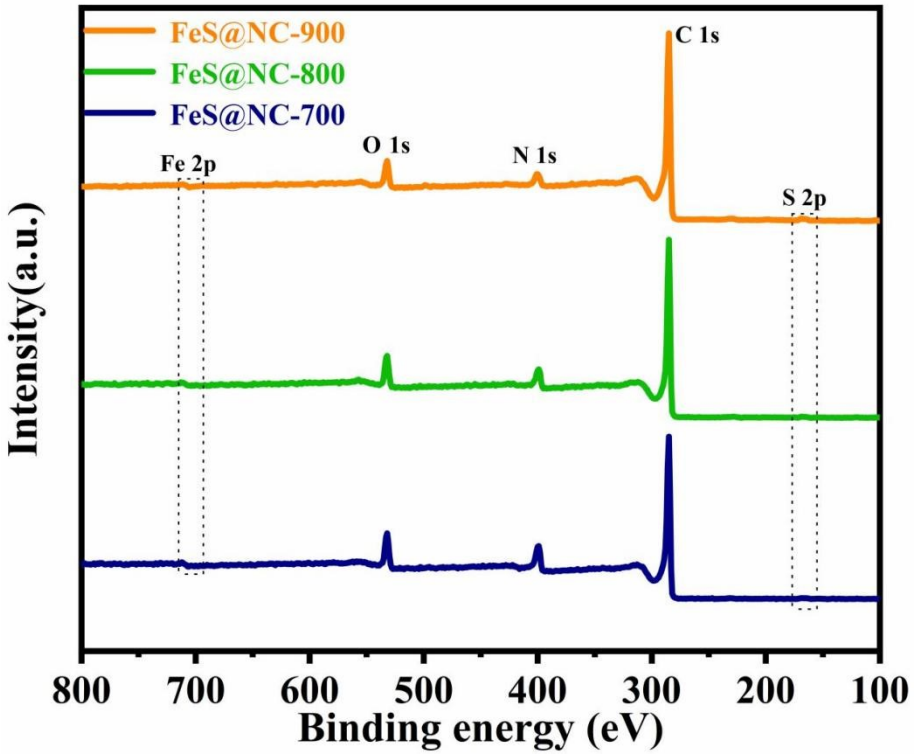

Figure S7. The full XPS survey spectra of FeS@NC-x (x=700, 800, 900).

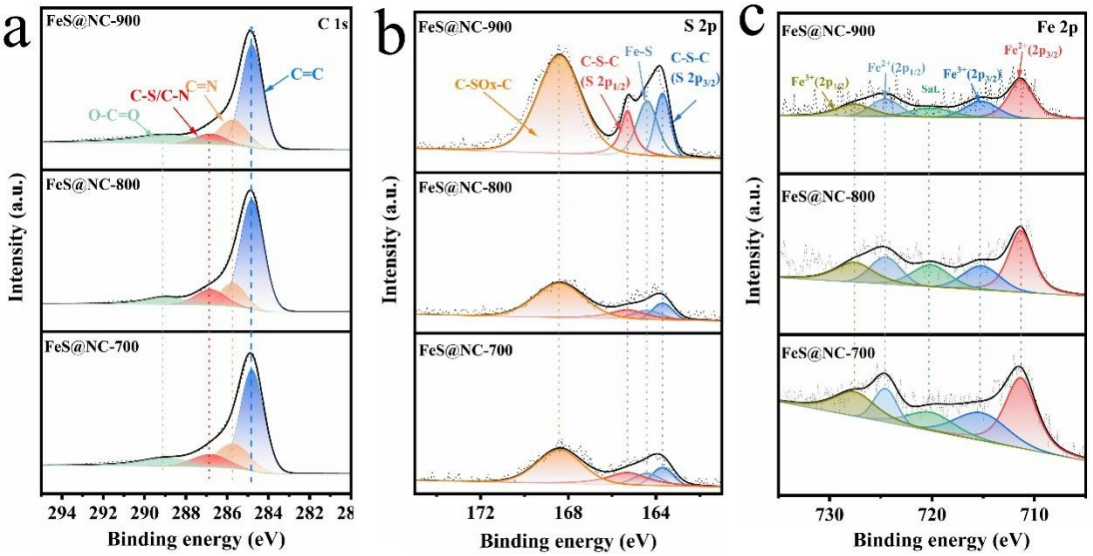

Figure S8. High-resolution XPS spectra of FeS@NC-x (x=700, 800, 900): (a) C 1s, (b) S 2p, (c) Fe 2p.

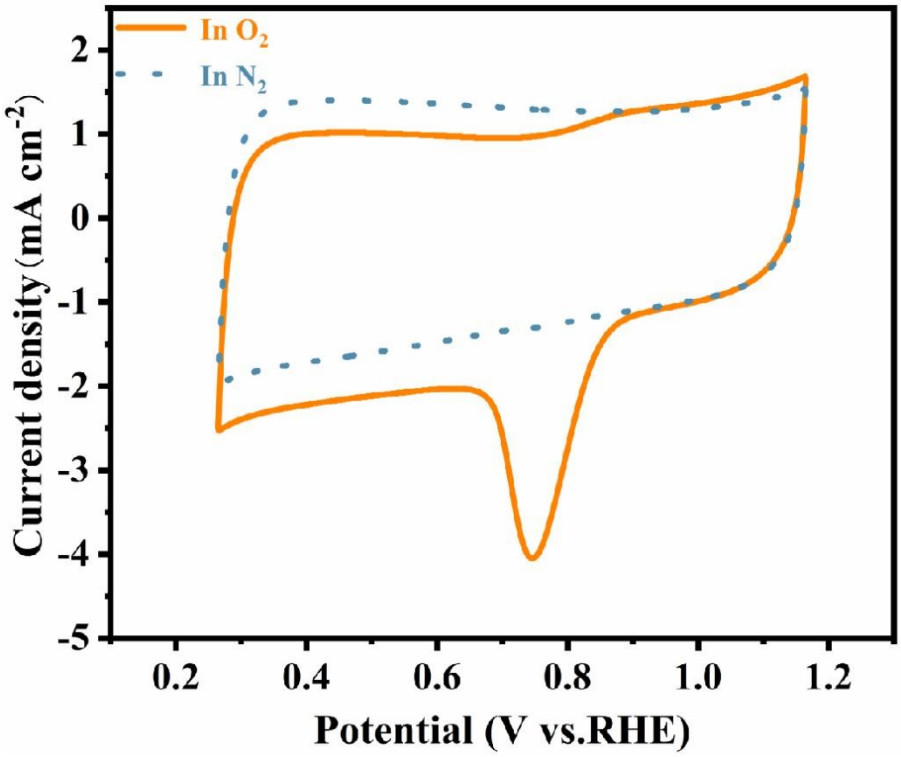

Figure S9. Cyclic voltammetry measurements of FeS@NC-900 tested in O_2 or N_2-saturated aqueous 0.1 M KOH.

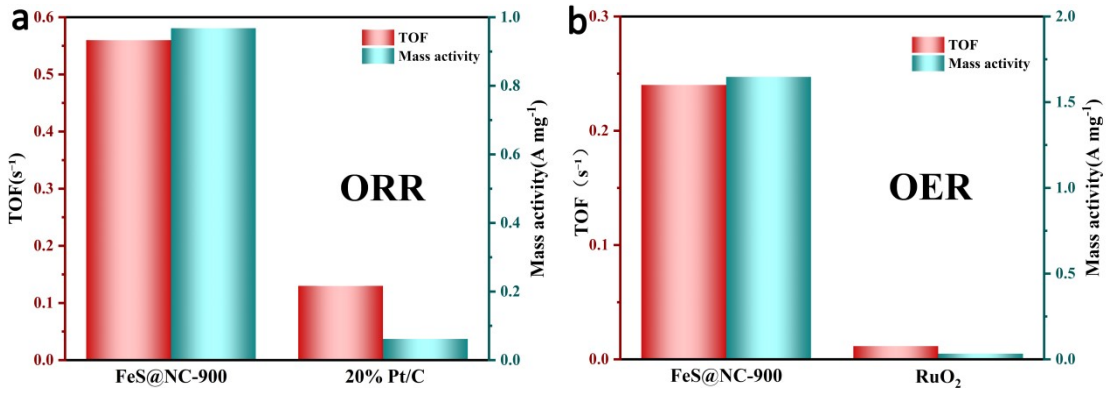

Figure S10. TOFs and mass activities of different samples: (a) ORR at 0.85 V vs RHE and (b) OER at 1.56 V vs RHE.

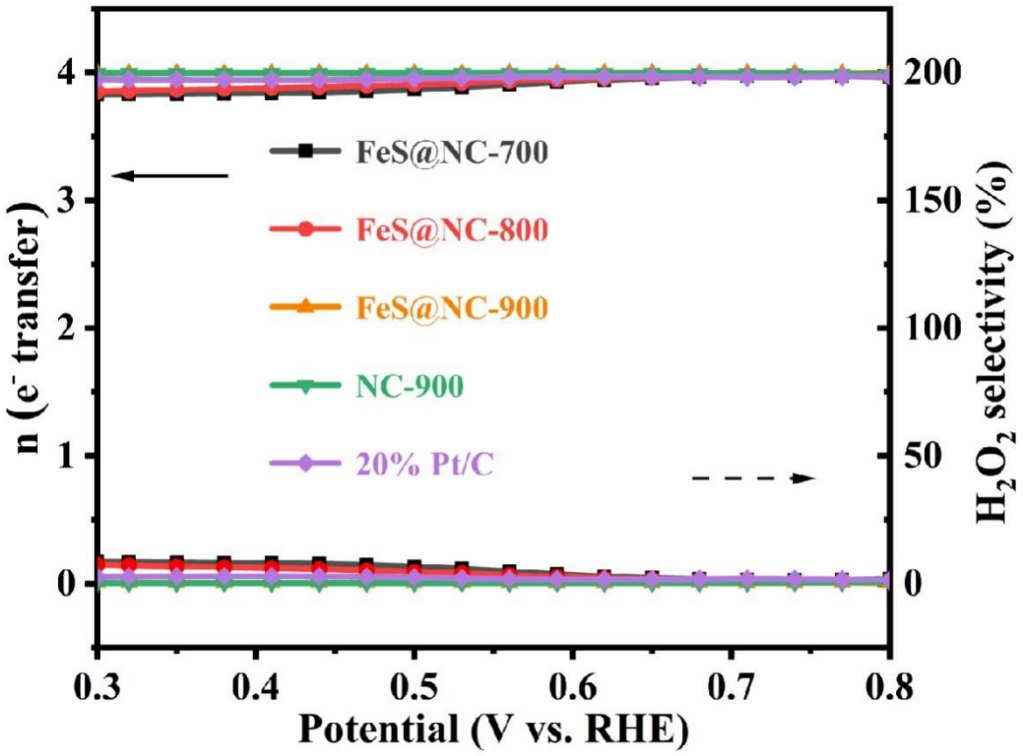

Figure S11. H_2O_2 yield and electron transfer numbers for different samples.

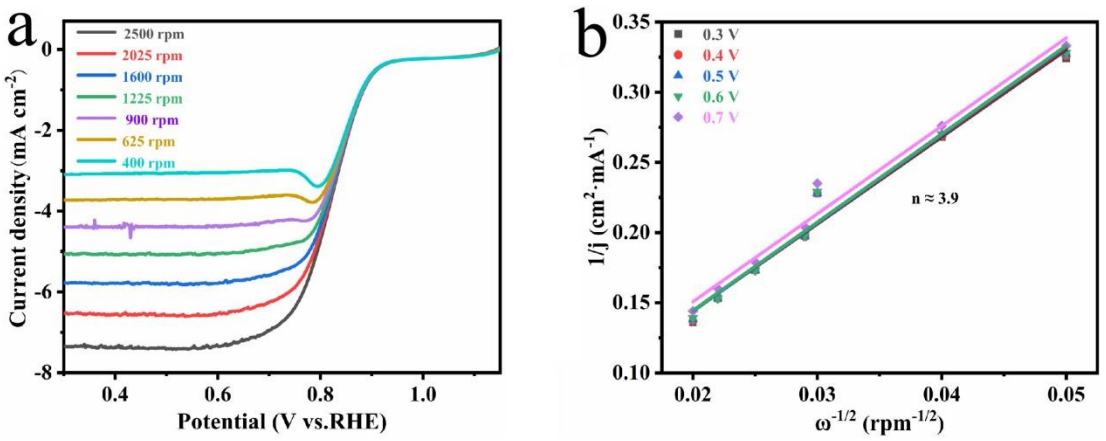

Figure S12. Polarization curves of FeS@NC-900 at the rotating speeds from 400 to 2500 rpm. (e) K-L plots.

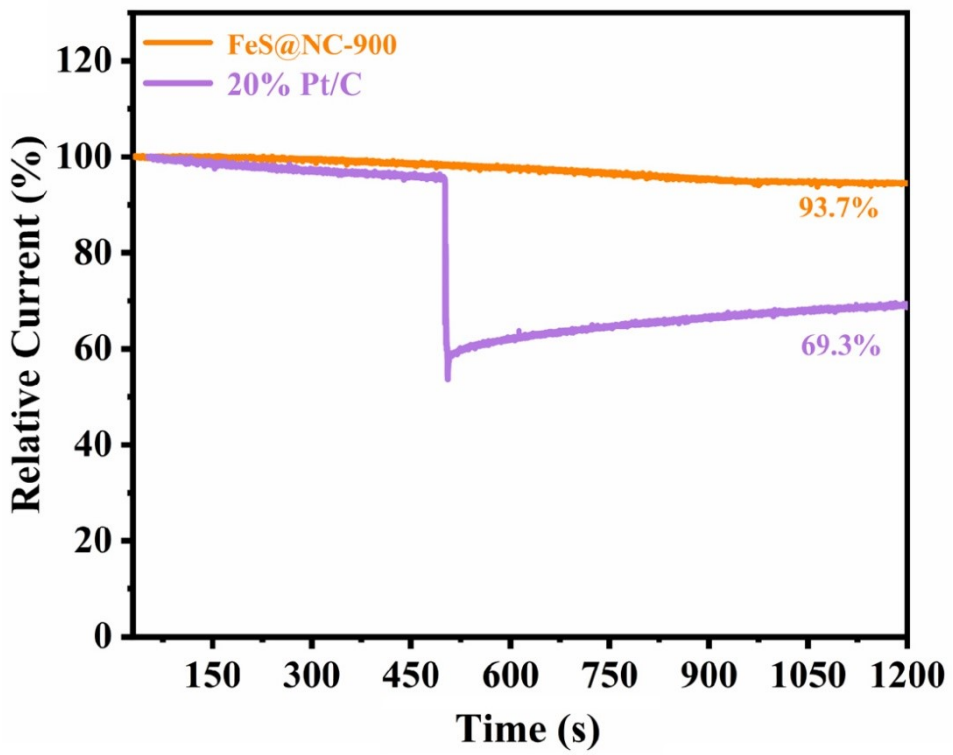

Figure S13. Chronoamperometric responses of FeS@NC-900 and commercial Pt/C before and after addition of 3 M methanol.

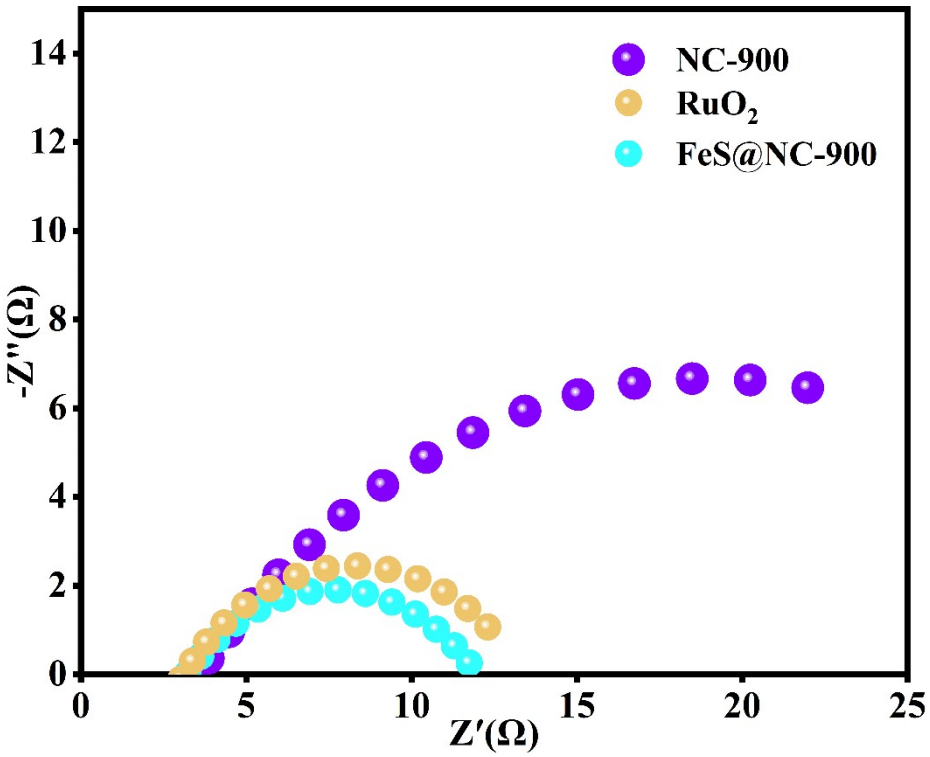

Figure S14. Nyquist plots of FeS@NC-900, NC-900 and RuO_2.

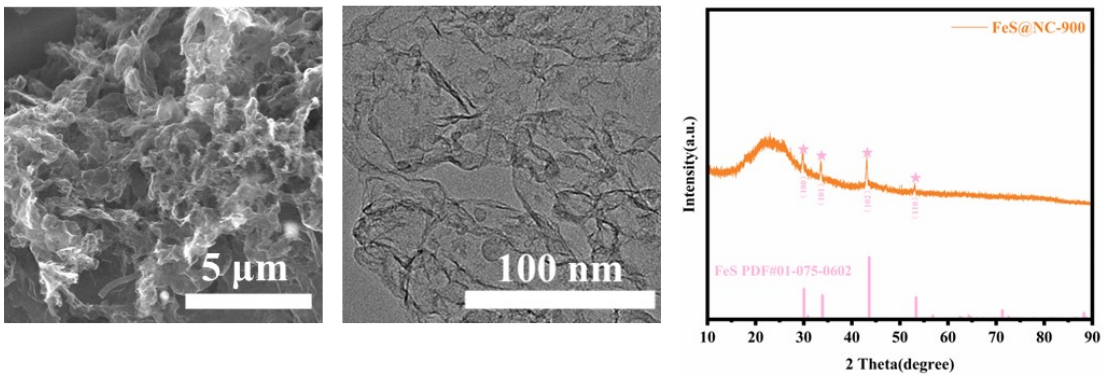

Figure S15. (a) SEM image, (b) TEM image and (c) XRD of FeS@NC-900 after stability test.

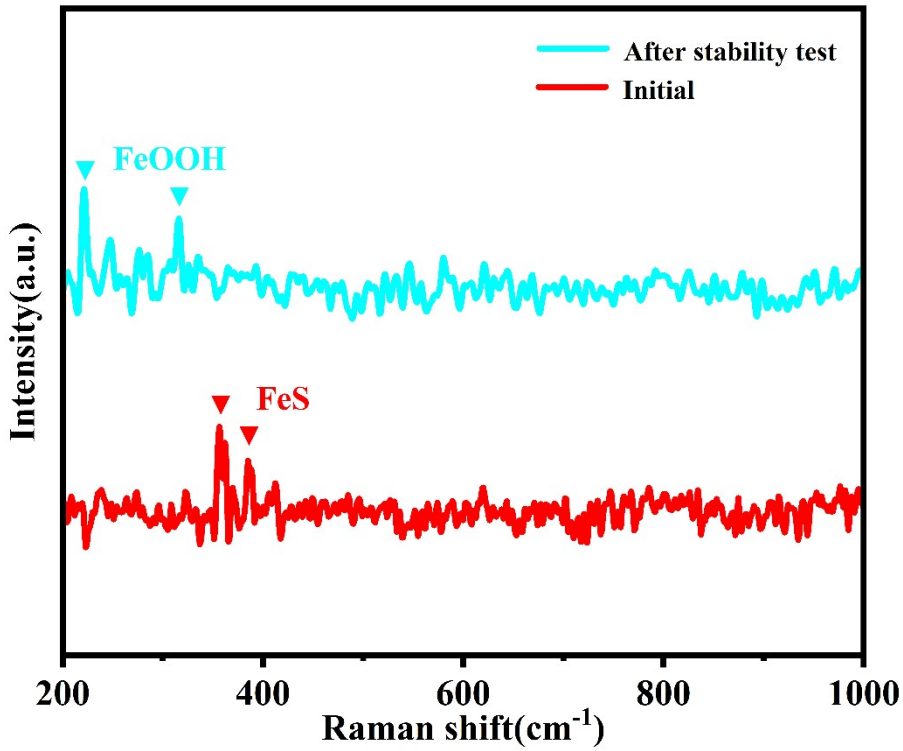

Figure S16. Raman spectra of FeS@NC-900 before and after OER/ORR cycling.

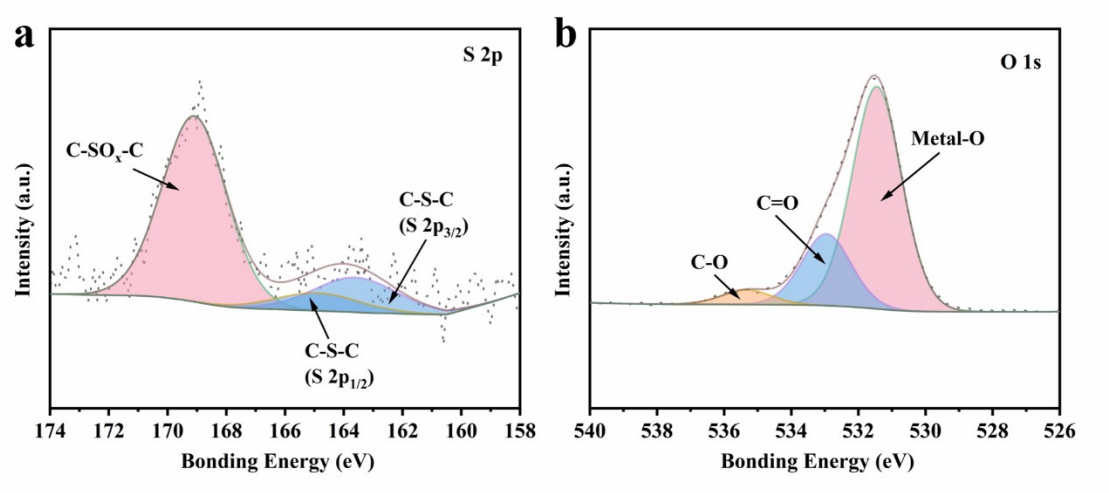

Figure S17. High-resolution XPS spectra of FeS@NC-900 after OER/ORR cycling: (a) S 2p, (b) O 1s

Table S1 The distribution percentages of various nitrogen states based on XPS.

Samples	Pyridinic-N (%)	Pyrrolic-N (%)	Graphitic-N (%)	Oxidate-N (%)
FeS@NC-700	37	31	23	9
FeS@NC-800	35	24	26	15
FeS@NC-900	30	18	36	16

Table S2. The comparison of bifunctional ORR/OER performance for FeS@NC-900 and other reported samples.

Catalysts	$E_{1/2}$ (V *vs*. RHE)	$E_{j=10}$ (V *vs*. RHE)	ΔE (V)	References
FeS@NC-900	**0.83**	**1.56**	**0.73**	**This work**
Fe_1Co_1@NC	0.85	1.564	0.714	**[S1]**
Fe/CoLDH@Co/NC	0.84	1.55	0.71	[S2]
Fe–Co_3O_4–S/NSG	0.77	1.51	0.74	[S3]
Ni/NiO-C	0.83	1.60	0.77	[S4]
Co_2P/Fe-Nx@NPC	0.835	1.54	0.705	[S5]
Co@NG-S2	0.798	1.66	0.862	[S6]
NiFe/WC@NC	0.81	1.52	0.71	[S7]
CoNi-NCNT	0.81	1.52	0.71	[S8]
Co–MOF/MX–1	0.81	1.59	0.78	[S9]
Co_3O_4/Ag NPs	0.75	1.47	0.72	[S10]

Reference

[S1] K. Lin, M. Chen, Z. Zhou, J. Zhang, Q. Wan, Z. Li, S. Peng, M. Sun, L. Yu, *J. Power Sources*, 2025, **641**, 236882.

[S2] N. Allwyn, S. Gokulnath, M. Sathish, *ACS Appl. Mater. Interfaces*, 2024, **16**, 19483.

[S3] L. Meng, Y. Wang, W. Liu, C. Fan, H. Nan, J. Wang, J. Yu, *Molecules*, 2023, **28**, 2221.

[S4] S. Rasaily, S. Chettri, D. Sharma, K. Baruah, R. Dewan, S. Tamang, A. Pariyar, *Inorg. Chem.*, 2024, **63**, 2856.

[S5] W. Liang, J. Shi, Z. Qin, J. Cai, Y. He, J. Li, *J. Alloys Compd.*, 2025, **918**, 180455.

[S6] C. Xia, H. Chen, D. Wang, S. Ding, *Electrochim. Acta*, 2025, **523**, 147607.

[S7] E. Jang, J. Cho, J. Kim, J. Kim, *Appl. Surf. Sci.*, 2024, **678**, 160201.

[S8] M. Qiao, Y. Wang, T. Wågberg, X. Mamat, X. Hu, G. Zou, G. Hu, *J. Energy Chem.*, 2020, **48**, 12005.

[S9] M. M. Mohideen, P. C. Santhosh, A. V. Radhamani, C. Wang, P. Hu, B. Subramanian, S. Ramakrishna, Y. Liu, *J. Colloid Interface Sci.*, 2025, **698**, 139165.

[S10] M. He, Z. Turup, W. Meng, M. Ding, Y. Li, T. Zhou, *Int. J. Hydrogen Energy*, 2025, **50**, 152912.